Microstructure- assisted changes in the magnetic Barkhausen emission of a mild steel under the influence of various mechanical and environmental loading factors; a semiquantitative analysis.

A .F. ALTZOUMAILIS [a*] , V. N. KYTOPOULOS [b]
[a*] School of Chemical Engineering, National Technical University of Athens, 5 Heroes of Polytechnion Avenue 157 73 Athens, GREECE.
[b]School of Applied Mathematical and Physical Sciences, National Technical University of Athens,5 Heroes of Polytechnion Avenue 157 73 Athens, GREECE.

Abstract: The aim of the present work is to introduce some novel possible ways for the semiquantitative analytical characterization of ferromagnetic steels. The characterization attempt focuses on microstructural changes occurring under the combined influence of certain mechanical loading as well as physico – chemical degradation factors such as applied stress-strain, tempering processing and salt water – induced electrochemical corrosion. In this direction, various conveniently simple developed functional modelling approaches are used to be able to analyse and estimate related experimental results obtained by means of micromagnetic Barkhausen emission measurements. The approaches are correlated to macroscaling as well as microscaling parameters such as stress-strain, dislocation – controlled cell size and pinning spacing – strength as well as internal cell flow stress. The needed correlations and estimations are made on the basis of an adopted specific micromagnetic activity parameter by which the obtained experimental data are compared and analysed. In this manner the opposite effects of internal flow stress and cell size reduction on the micromagnetic activity can reasonably be demonstrated where the first tends to stimulate an increase while the second a decrease in the specific micromagnetic parameter with progressive plastic deformation. One can further demonstrate that various physico-chemical degradation factors may markedly influence the microstructural as well as micromagnetic behaviour. For instance, hydrogen produced by corrosion of steel in NaCl – water solution and tempering processing lead to appreciable mechanical embrittlement as well as magnetic hardening of steel, expressed by an associated decrease in the specific micromagnetic parameter. With respect to this the tempering processing leads to a higher magnetic hardening compared to the corrosion process of steel.

Key Words: Micromagnetic activity, J-parameter,cell – size, cell flow stress, q- factor, strain, pinning spacing- strength, dislocation, domain wall, mobility.

Received: May 9, 2021. Revised: June 25, 2022. Accepted: July 21, 2022. Published: September 14, 2022.

1. Introduction

Physical and mechanical characterization of structural steels by non-destructive techniques may become vital for assessment of proper initial heat treatment and subsequent degradation of microstructural and mechanical properties of steel elements exposed to in service conditions such as creep, static or cyclic loading. With respect to this, micromagnetic Barkhausen emission (MBE) is widely used as a basic characterization technique for structural steels [1-16]. Nevertheless, the underlying magnetization process in magnetic materials has been an important and difficult research subject for many years because of a lot of factors contributing to the process. This can be described on both macroscopic and microscopic scales and analysed by different methods, such as magnetic hysteresis loop, which is mainly representative of macroscopically – averaged magnetization

events, as well as by MBE describing various microscopic physical properties of material and including its local mechanical state. It is interesting to note the significant fact that the MBE provides a non – destructive information on the state of a magnetic material which is independent of that obtained by bulk magnetic techniques such as hysteresis. It is well- known that magnetization processes in ferromagnetics are strongly influenced by the stress-strain state of material under activation of micromagnetic phenomena determined by the domain wall dynamics [11-12]. For instance, plastic deformation gives rise to regions of high dislocation density which due to long-range stress field interaction, may impede domain wall motion. Elastic stress also affects the MBE because of the magnetoelastic coupling effects. By these effects domain magnetization tends to align with an easy crystal axis lying closer to the direction of stress axis and as such to stimulate an increase in the MBE-rate.

The MBE can be detected as electric voltage pulses induced by abrupt- discontinue changes in magnetization which are the result of irreversible domain wall motion between pinning obstacles (sites). The type of obstacles which act as energy barriers to domain wall motion may be grain boundaries, dislocation arrays, voids, microcracks, stress gradients, precipitations and other microstructural defects or discontinuities.

Today, various, more or less sophisticated magnetic testing techniques are used to characterize many types of structural steels [10]. However, due to the complexity of data interpretation, view of these techniques are used for a more easy and practical characterization of steels under combined influence of applied stress and various physico- chemical degradation factors [5,8,13,14]. In this sense a correct explanation and interpretation of data for materials tested under conditions of combined progressive plastic deformation and various environmental degradation factors, become a complex task. Under these conditions, for instance, the superposition of residual and applied stress becomes competitive with peculiar, internal physical factors, resulting in an unexpected mechanical strength degradation of steel. The present work focuses on a more or less semiquantitative characterization of MBE-response of a mild steel under the combined influence of applied stress and various thermal and electrochemically corrosive environmental loading factors. This task is performed on the basis of appropriate modelling approaches by which relevant characteristic parameters are introduced and their adequacy and reliability analysed and discussed. Nevertheless, one must be very careful in this attempt because there are some difficulties which researchers experience to study the MBE phenomenon. These are mostly related to the very sensitive nature of the emission to microstructural changes in material. Furthermore, a small change not only in one of the microstructural parameters but also in one of the generating or detecting parameters of the emission of an experimental set up may result in additional challenges to interpret in a correct way the obtained results [16].

2. Theoretical Background

2.1. Basic Assumptions

A general form of specific potential energy of domain wall in form of

$$E_p = \frac{1}{2}a_0(s-s_0)^2 + a_2(s-s_0)^4 + a_3(s-s_0)^6 \ldots\ldots + a_i(s-s_0)^{2i} \quad (1)$$

can be assumed, where by definition a stable, minimum energy location S_o may by chosen. The desired specific domain wall energy stored in the unit area of crystal lattice, a*, is given as:

$$\gamma = \pi \cdot (A\,K_1/a^*)^{1/2} \quad (2)$$

Now, by taking in Eq. (1) $a_0 >> a_i$ (i>0), one can obtain an approximated form of potential energy given by [12]:

$$E_p = \frac{1}{2} a_o s^2 \propto \gamma \quad (3)$$

where A is the exchange energy constant and K_1 the cubic magnetocrystalline anisotropy constant. The magnetic energy is assumed to be changing with the related displacements of the wall, [12].

$$E_H = -2I_s \cdot H \cdot s \cdot cos\vartheta \quad (4)$$

The total energy has the form

$$E = E_p + E_H = \frac{1}{2} a_0 \cdot s^2 - 2I_s \cdot H \cdot s \cdot cos\vartheta \quad (5)$$

Here I_s is the saturation magnetization, H the applied magnetization filed and θ the angle between the direction of applied filed and domain wall magnetization.

By this, from the condition of minimizing the free energy, results:

$$\frac{\vartheta E}{\vartheta s} = 0 = a_0 s - 2I_s \cdot H \cdot cos\vartheta \quad (6)$$

and further

$$s = \frac{2I_s cos\vartheta}{a_0} \cdot H \quad (7)$$

This relationship may tentatively be seen as a condition of a probable transition from a reversible to an irreversible jump motion of domain wall in overcoming the potential energy of pinning sites (abstacles).

Now Eq. (4) becomes:

$$|E_H| = \frac{4I_S^2 \cdot H^2 cos^2\vartheta}{a_0} = I_\vartheta \cdot H \quad (8)$$

Further we put:

$$I = \frac{4I_S^2 cos^2\vartheta \cdot S^*}{a_0} = I_\vartheta \cdot S^* \quad (9)$$

Where I=total magnetization, I_θ = angular magnetization and $S^* = \frac{l_x^2 + l_y^2 + l_z^2}{l_x l_y \cdot l_z} = 3/L$

is the specific wall surface or total area of 180 ^{0}- walls included in a unit volume provided that the internal stress fluctuates with same intensity in the x, y, and z directions

$(l_x l_y = l_z = L = operationalconstant.)$ [12].

When the angular distribution of domain magnetization is isotropic, than one can calculate

$$\int_o^{\pi/2} cos^2\vartheta \cdot sin\vartheta \, d\vartheta = \overline{cos^2\vartheta} = \frac{1}{3}$$

and Eq. (9) becomes

$$I = \frac{4}{3} I_s^2 \cdot H \cdot 3/l \cdot a_o = 4I_s^2 \cdot H/L \cdot a_o \quad (10)$$

Here a_0, is the potential strength or gradient factor given as:

$$a_0 = \frac{\vartheta^2 \gamma}{\vartheta s} \quad (11)$$

Furthermore, it is known that the voltage signal, induced and detected in the experimental magnetizing set up, is given by the induction law given as:

$$\frac{dB}{dt} = \frac{dI}{dt} + \mu_0 \frac{dH}{dt} = V_{rms} \cdot C_0 \quad (12)$$

Where C_0 is an electronic processing accommodation constant and Vrms the root-mean-square voltage measured over given magnetization cycles.

Finally, one may estimate as: $4I^2_S/L$. $a_0 >> \mu_0$

And Eq. (12) becomes:

$d\beta/dt = dI/dt = V_{rms}.C_0$ (12a)

2.2 Preparative approaches

During plastic straining a cell-structured dislocation array develops by a decrease in the related cell size. An associated effective internal cell flow stress field develops equivalent with the local stress field (seen) by mobile dislocations moving through the "forest" - sessile ones. In this manner the applied effective stress results from superposition of elastic and (shear) flow stress concentrated around cell walls. Thus, the magnetic walls are more likely to interact with forming cell walls rather than with individual dislocations since effective

internal stress is almost proportional to the absolute value of internal stress depending on the microstructure of dislocation network. In this sense the major obstacles in form of pinning sites to the motion of domain walls appear to be dislocation tangles localized within the cell walls and/or grain boundaries. Single defects, like isolated dislocations can interact with small domain wall displacements, mostly in the so-called Rayleigh region of hysteresis.

Thereafter, the wall motion can be approached by assuming, in a first instance, a_o=constant, which means that the strength of potential wall does not change with time of domain wall motion. At the same time, it is advisable to introduce a simple form of an operative, highly localized cell (grain) stress field given by periodic variations as expressed by [12]:

$$6_s = 6_0 cos 2\pi \frac{s}{\tilde{l}} \quad (13)$$

Here, $\tilde{l}$is the average wave length of spatial (planar) variation and σ_0 the amplitude of this field (see also Appendix-A). The existence of this field could be substantiated by the fact that it may reasonably be correlated to with the internal flow stress-aided formation of dislocations tangles-structured cell walls [9] (see also Appendix-A). Furthermore, the Eq. (13) takes into consideration the existence in the material of localized, long-range, statistical thermoelastic stress fluctuations [10] which, in turn, may cause respective fluctuations in the domain wall pinning energy, fact coupled through Eq. (13) and (14), with a decrease in the K_{eff}. Thus, thermoelastic changes-stimulated irreversible wall displacements may also contribute to a net increase in the micromagnetic activity – determined MBE. Moreover, one can reasonably assume, in a "Zeroth" approximation, the validity of the expression: $\tilde{l} = l$= effective pinning spacing which would determine the effective mean-free path length of moving domain wall. Thus, by means of the sketch of Fig (1) one may argue that Eq. (13) describes a stress state, developed between pinning sites as given by $6_0 = 6_s(s \to 0)$ and $6_0 = 6_s(s \to l)$ conditions determined by cell size and/or grain boundaries. In this approach it is assumed that domain walls initially may "oscillate" between these pinning barriers having a probability to overcome these barries and consequently to move irreversibly giving a Barkhausen event. In general, it is pointed aut that the above introduced internal stress field should be considered as an effective, highly localized one, affecting the mobility of magnetic walls, rather than an internal field in the usual sense

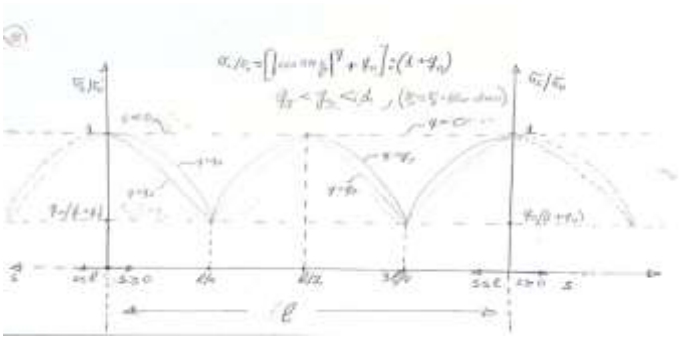

Figure 1: Sketch of internal cell flow stress distribution.

Thus, the existence of such a field leads to a reduction in the effective magnetocrystalline anisotropy constant as given by [12]

$$K_{eff} = K_1 - \frac{3}{2}\lambda \cdot 6_s \quad (14)$$

thus increasing the micromagnetic emission activity; λ is the saturation magnetostriction constant.

In inserting Eq. (14) into Eq. (2) one obtains:

$$\gamma = 2\sqrt{AK_1}\left[1 - \frac{3}{2}\frac{\lambda 6_s}{K_1}\right]^{1/2} = 2\sqrt{AK_{eff}} \quad (15)$$

Thereafter, by means of Eqs. (15) and (11) one may calculate the potential strength constant a_0. Since the needed algebra of approximation steps is somewhat lengthy, these are given in the unpublished data of the authors [17]. So, it can be shown that: $a_0 \approx constant. \cdot 1/l^2$

2.3 Uniform wall motion

In the next second approach we introduce a more general formulation of cell flow stress compared to Eq (13):

$$6_s = \frac{6_0}{1+q_0}\left[\left|cos\frac{2\pi s}{l}\right|^q + q_0\right] \quad (16)$$

Here, q and q_0 are applied stress-dependent parameters, where q should decrease while q_0 increase with applied remote stress6_∞. The essence of this field is illustrated in the sketch of Fig (1). More concrete, q arises to be a stress field shape – strength number and q_0 an overall stress field shift number.

It is mentioned that the wave length,$\tilde{l}$, or pinning spacing l in Eqs (13) and (16) should obey the condition$l_g \geq l \geq l_c$, where l_g is the average grain size (diameter) and l_c the average cell size (diameter). Furthermore, one may put:

$$\gamma \propto \sqrt{AK_{eff}} \quad (17)$$

By virtue of Eq (15), Eq (16) and Eq (17) it follows

$$\gamma = 2\sqrt{AK_1}\left\{1 - \frac{6_0}{1+q_0}\frac{\lambda\cdot 3}{K_1\cdot 2}\left[\left|cos\frac{2\pi s}{l}\right|^q + q_0\right]\right\}^{1/2} \quad (18)$$

Using Eq (11), one may evaluate the potential strength number a_o and as such after executing the needed algebra of approximation steps, as shown in [17], one obtains

$$a_o = \frac{2\pi^2}{L}\frac{\lambda\cdot\delta}{K_1}\left(\frac{q}{1+q_0}\right)\cdot\left(\frac{1}{l^2}\right) = constant \cdot \frac{1}{l^2}\left(\frac{q}{1+q_0}\right) \quad (19)$$

Consequently, from Eqs (10) and (12a) it follows:

$$V_{rms} = \frac{6_\infty}{6_y}l^2\cdot\left(\frac{1+q_0}{q}\right)\cdot constant = const.\frac{6_\infty}{6_y}l^2\cdot\tilde{q} \quad (20)$$

Here, $\tilde{q} = (1+q_0)/q$ is an adopted cell (grain) flow stress elevation factor. Again, as shown in the sketch of Fig (1), the parameter q_0 increases, whereas q decreases with applied stress, fact which would lead to a contribution to a rapid increase in this factor and consequently in the detected Vrms voltage signal of the above equation. It should in other words be mentioned that the existence of the above flow stress elevation factor, $\tilde{q}$, may stimulate, in several ways, a transition from a reversible to an irreversible domain wall jump motion. This can be substantiated, primarily, by the fact that in a highly stressed-strained ferromagnet material the magnetoelastic second-order coupling interaction coefficient becomes larger than standard values [11]. In this way, the resulting (strong) magnetoelastic intercell (intergrain) coupling effect would increase the volume of correlated magnetic domain regions and hence the number of (large) jump events. This, in turn, would produce an increasing V_{rms} voltage measured in the experimental set-up. Moreover, with further contribution of other effects of stress-controlled domain wall dynamics [11], the height of pinning energy barriers may appreciably be lowered in further increasing the micromagnetic activity- determined MBE rate.Nevertheless, in connection to the above statements, it is mentioned that the internal flow stress, initially, may opposites to the movements of magnetic walls and reduce the MBE. This would be expressed by a reduction in the wall mobility, reflected by a shift of a given measured count rate to higher magnetizing fields. Generally, this would mean that an increase (decrease) in the wall mobility can be correlated with an overall shift of a given emission rate to lower (higher) applied magnetic fields. However, as demonstrated in a recent study by the authors [15], local flow stress may exhibit an indirect, "hidden", stimulating effect on the wall mobility in the sense that it may lead to an appreciable increase in the pinning strength (force) correlated to with a dominating rate of increase in the wall start acceleration. As such, due to the kinematic counterbalance of changes of all variables in equations $l = \tilde{\alpha}t^2/2$ a net increase in the average wall

velocity may result in increasing the measured V_{rms} signal. Furthermore, with respect to Eq (9) and Eq (14), results that the primary effect of an increased internal (flow) stress field , concentrated around defects, such as dislocation tangles-structured cell walls as given by relationship $6_s \rightarrow 6_0 \rightarrow 6_f$ and shown in Fig(1) leads to a reduction in the local magnetic anisotropy constant towards an effective one, K_{eff}, as expressed by Eq (14).

This, in turn, would create an effectively lowered pinning energy barrier to domain wall motion resulting in an increase in the micromagnetic activity. However, there are many vague points about the distribution of internal (flow) stresses and since, in addition, the magnetostriction is basically anisotropic, so the magnetic antistropy induced by such stresses would be fairly complicated. Furthermore, it is assumed, in a first approximation, that the measured count rate, N, may be expressed by simple functional relationships as follows (see also Appendix-B):

$$N_m = \left(\frac{6_\infty}{6_y}\right) \cdot \xi_o \cdot [1/l^m] \qquad (21)$$

$$N_p = \left(\frac{6_\infty}{6_y}\right) \cdot \xi_o \cdot \left[1/l^{1/p}\right]^{\xi_{m.p}} \qquad (22)$$

with $N_m = N_p = N$= measured count rate. Here, $m = f_m(l)$= mobility number as a function of pinning spacing, l, and $p = f_p(l)$= pinning strength number as a function of, l; ξ_o is a set-up constant. As such, results that $f_m(l) \cdot f_p(l) = \xi_{m,p}$= microstructural pinning state accommodation constant and ξ_o is a macroscopic accommodation measuring constant (6_∞ and 6_y are the remote applied stress and yield stress respectively). It is noted that the relationships (21) and (22) would numerically ensure the existence of the experimentally established suppressed – equilibrated parabolic increase in the measure count rate, N, [8]. This could be attained by a balanced – competitive decrease in the both parameters l, m of Eq (21).

In this context and for the sake of consistency with the reality of experimental findings [8] one may postulate as follows: an increase in the plastic deformation would lead to a decrease in the wall mobility number, m, and an increase in the pinning strength number, p. Thus, two extreme conditions of microstructural pinning state may exist: first, $l \rightarrow l_{lim}^{+}$, $p \rightarrow p_{lim}^{+}$, $m \rightarrow m_{lim}^{+}$ and second $l \rightarrow l_{lim}^{-}$, $p \rightarrow p_{lim}^{-}$, $m \rightarrow m_{lim}^{-}$. Here,$l \rightarrow l_{lim}^{+}$, $p \rightarrow p_{lim}^{+}$, $m \rightarrow m_{lim}^{+}$ are the characteristic upper limit of the related parameters whereas $l \rightarrow l_{lim}^{-}$, $p \rightarrow p_{lim}^{-}$, $m \rightarrow m_{lim}^{-}$ the characteristic under limit of the same parameters. Therefore, the first condition simulates a tendency to a hard whereas the second one a tendency to a soft magnetic material. Furthermore, the first condition would simulate a micromagnetic activity controlled by large number of small jump events whereas the second one an activity controlled by small number of large jump events.

Concerning Eqs (20), (21) and (22) it is further mentioned that the presence of " empirical" macroscaling stress factor$\frac{6_\infty}{6_y}$, in the above equations could be substantiated by the experimental findings presented in Fig (2), where the measured count rate, N, and V_{rms} signal show similar trend of behaviour with applied stress. In this context one may roughly assume that N≈ constant. n, where n= pinning sites density. This assumption would be valid for the same, given instant conditions.

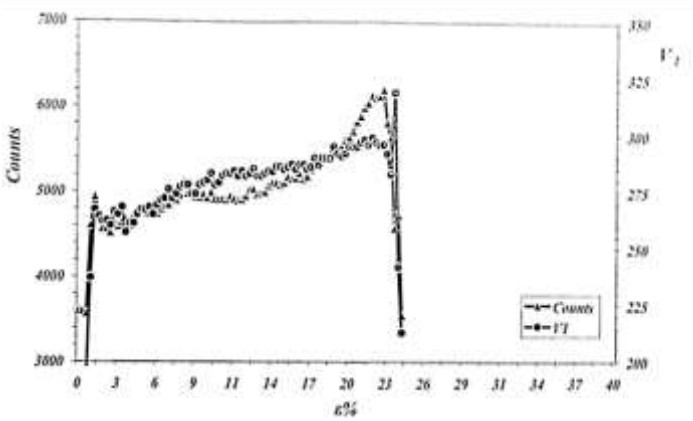

Figure 2: plot of the Barkhausen emission signal of count and volte respectively.

Now, by introducing the specific micromagnetic activity (s.m.a.) parameter $J = V_{rms}/N$ as a basic measuring and analysis parameter [5, 13-15] one obtains through Eqs (20) and (21):

$$J = constant(l^{2+m} \cdot \tilde{q}) \qquad (23)$$

It is emphasized that the above proposed specific parameter results essentially to be a microscaling, applied stress-independent variable. In this manner the influence of (nominal)-macroscaling applied stress on the micromagnetic activity is practically "decoupled" from the internal-microscaling (flow) stress variable and as such, the above-proposed specific activity number J would reflect the sole influence of the latter. In addition, due to the relative strong functional dependence on, l, the above parameter seems to be (very) sensitive to small microstructural changes occurring in the material.

2.4 Non-uniform wall motion

By this approach the existence of a finite variable of wall jump velocity V_w is assumed. This fact can be connected with the more general assumption that the potential strength,a_o may change with time of wall motion. On combining Eqs (10) and (12a) we get:

$$\frac{dI}{dt} \cong \left[\frac{1}{a_0} \cdot \frac{dH}{dt} + H \cdot \frac{d}{dt}\left(\frac{1}{a_0}\right)\right] \cdot \frac{4I_S^2}{L} \qquad (24)$$

Taking into consideration Eq (19) and following the approximating steps given in [17] one obtains

$$\frac{dI}{dt} = \frac{4H \cdot I_S^2 \cdot V_w \cdot l}{\pi^2 \cdot \delta \cdot \lambda \cdot L}\left[\left(\frac{1-q}{q}\right) \cdot (q_0 + 1)\right] = constant. \left[l \cdot \left(\frac{1-q}{q}\right) \cdot (q_0 + 1)\right] \qquad (25)$$

Now, we adopt a kinematics approach where the wall velocity V_w is a variable with time i.e. $V_w = \tilde{a}t$ and $\tilde{a}$ is the constant wall start acceleration.

Further it is$l = \tilde{a} \cdot t^2/2 = V_w \cdot t/2$, where by elimination of time, one obtains$V_w = \sqrt{2\tilde{a}l}$. As such, from eqs (25) one may have [17]:

$$V_{(rms)} = constant. \left(l^{\frac{3}{2}} \cdot \tilde{q} \cdot \frac{6_\infty}{6_y}\right) \qquad (26)$$

Here, $\tilde{q} = \left(\frac{1-q}{q}\right)(q_o + 1)$ is the new adopted cell (grain) flow stress elevation factor. It is interesting to note that the ratio of this factor to that of Eq (23) becomes proportional to 1-q which should increase with applied stress (plastic deformation). This means that the non-uniform wall motion approach compared to the uniform one simulates a stronger stress elevation factor effect in increasing the measured voltage signal. Thus in a similar procedure as for Eq (23) we obtain:

$$J = constant\left(l^{3/2+m} \cdot \tilde{q}\right) \qquad (27)$$

2.5 Bulging-coupled wall motion

By this approach we taken into consideration the possible, finite, bulging displacement (deflection) of pinned - fixed domain walls ass observed experimentally in [18] and shown in the stretch of Fig (3).

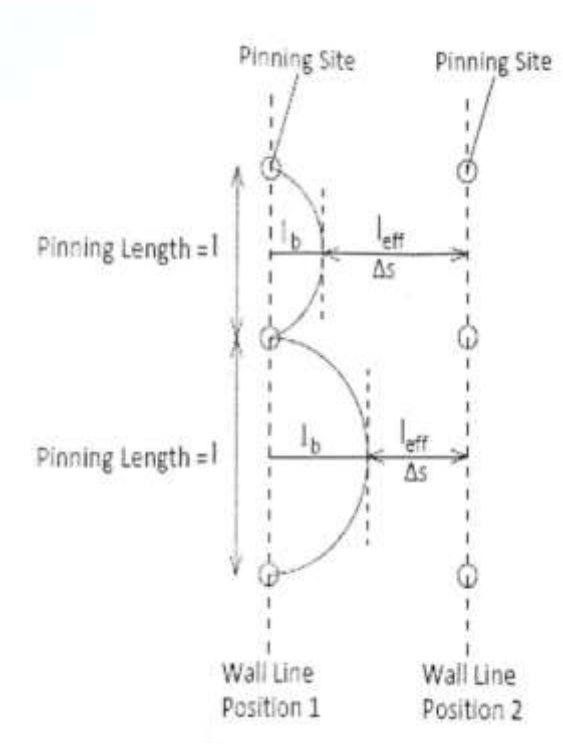

Figure 3: Schematic Presentation of wall motion by bulging displacement

We define$l_{eff} \propto (l - l_b)$, where l_{eff} is the effective wall displacement l the pinning spacing and l_b the current bulging length. In

addition, we define the current changes in the effective wall displacement as $\Delta s \rightarrow \Delta l_{eff} = \Delta(l - bl) = \Delta l(1 - b)$ where $0 \leq b \leq 1$ is a bulging strength number. Thereafter, the final form of the needed specific micromagnetic activity parameter becomes:

$$J = constant[l \cdot (1 - b)]^{3/2+m} \cdot \tilde{q} \quad (28)$$

or in a simpler from

$$J \propto l_{eff}^{3/2+m} \cdot \tilde{q} \quad (29)$$

At this place it is mentioned that tensile stress applied in the direction of magnetic field favors the growth of longitudinal-basic magnetic domain in suppressing the existing transverse-supplementary ones, anchored on the first. Otherwise, without applied stress, the transverse-supplementary (secondary) domains, due to the magnetostrictive friction effects, would exhibit an increasing pinning energy barrier to the movement of the basic domains. This would mean that under applied stress conditions and hence by an increase in the cell (grain) flow stress elevation factor ($\tilde{q}$) and for the same pinning sites, the wall membrane may execute reduced bulging deflections reflected by associated small bulging strength number, b, fact witch according to Eq.(10) would lead to an increase in the specific parameter, J. In general, concerning the relationships (27) and (28) it should be noted that the complex interplay between the opposite effects of a decrease in pinning spacing, and a decrease in wall mobility number, m, as well as an increase in the $\tilde{q}$ – stress factor with plastic deformation, should lead to the final net value of the desired J – parameter.

3. Experimental Procedure

A block diagram of the experimental set up used for the measurement of micromagnetic Barkhausen emission (MBE) is shown in Figure 4. More details about the measuring technique can be extracted from Ref.[5,13-15] The specimen had dogbone – type geometry where thickness was 2mm, width 10mm and the effective gauge length 100mm. The samples were subjected to uniaxial tensile test at room – temperature and nominal low strain rate 10-4/s, using a universal testing machine of Intsron – type. The ultimate stress was 380 MPa and the yield stress (0.2% offset) was 190MPa. Before testing, the samples were exposed to a corrosive environment produced by a continuously sprayed 3.5% NaCl aqueous solution. All corrosion experiments were performed at room temperature ($25C^0$). The exposure time were 200, 400, 600, 800, 1000 hours. The final corrosion product formed on the specimen surface was in a greatest part, as obtained by X- ray diffraction analysis, a ferric oxyhydroxide (FeO-OH) component. The produced corrosion layer was removed by dry air blast and soft natural bristle brush revealing underneath a black and strong adhering. It is pointed out that during the corrosion production of atomic hydrogen takes place by the basic electrochemical reactions [13]. Tempering process of specimens was conducted by means of air ambient heated at temperature $440C^o$. After tempering the specimens were cleaned by appropriate etching to remove any eventually formed oxjdation layers.

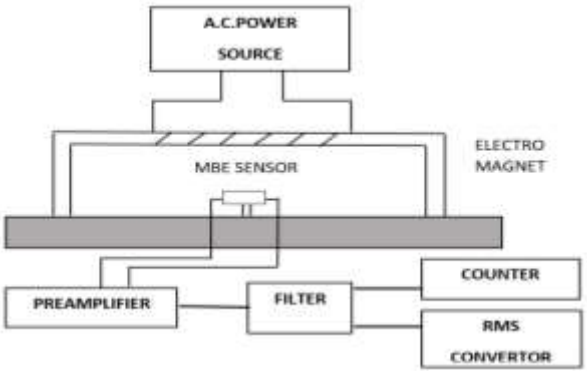

Figure 4. Schematic of Block diagram of used magnetic Barkhausen set up.

C	Mn	Si	Ni	Cr	Mo	S	P	N
0.05	0.44	0.015	0.016	0.015	0.002	0.016	0.02	0.004

Table1. The chemical composition of used low-carbon steel

4. Results and Discussion

In previous works [5, 13-15] the authors have introduced the J-mode of analysis by means of the adopted specific micromagnetic activity (s.m.a) parameter J. The advantages of this mode of analysis are explained in details in the mentioned works. Following this mode of analysis the Fig (5) is presented, where for sake of practical discussions the stress-strain curve and corresponding magnetic J-strain curve of as received (virgin) material are plotted together.

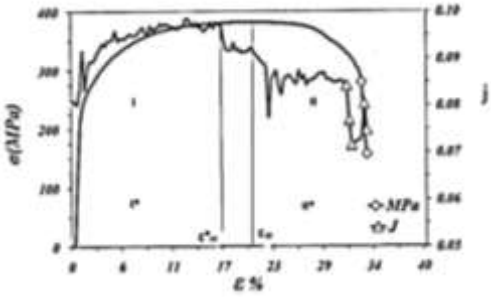

Figure 5: Applied tensile stress and specific ME-response parameter plotted against operative strain for initial, corrosion (hydrogen) free condition.

In this Figure an almost "simultaneous" increase in both curves with strain up to a certain strain point can be observed. This point coincides with the ultimate tensile strength determined by the plastic instability of necking formation in the material. Beyond this strain point both curves decrease continuirly up to final fracture. Let this point be seen as a critical strain, $\tilde{E}_{cr}$ characterized by development of triaxial tensile stress field resulting in the creation of internal damage sites in form of microvoids, microcracks dimples and cavities which may growth and coalesce leading to final fracture. Thereafter, as shown in [13, 14], it can be assumed that this critical point separates the evolution of the stress-strain as well as J-strain curve in two basic-distinctive regions; a prenecking (I,I*) and a postnecking (II,II*) region. At the same time, one can observe that the evolution of the magnetic J-strain curve is characterized by numerous small and/or large changes in form of consecutive minima and maxima occurring in the material. For instance, the initial-linear increase in the J-curve observed up to the strain point of about 1%,in the magnetic prenecking region I* ,suggest to assume a dominant contribution of the stress elevation factor q in stimulating, as shown by Eqs (27) and (28), a linear increase in the s.m.a. number J. This strong dominance is corroborated by the fact that up to this point a more or less homogeneous distribution of low-density dislocation arrays exists. This would mean a relative small changes in the average pinning spacing, l, or density and as such, according to Eq (27), this would have a negligible influence on the J-number. Beyond the 1% strain point the J-curve is characterized as mentioned by formation of consecutive abrupt steps of minima/maxima. This is because beyond this strain point a cell-structured network develops rapidly in reducing the cell size and hence the effective pinning spacing, l, fact which according to Eq (27) and (28) tends to reduce the J-number. Thus, in other words, the oscillating opposition of the $\tilde{q}$-factor effect and pinning spacing l-effect leads to formation of the above-mentioned consecutive-equilibrated maxima/minima steps in the J-strain curve.

Bearing in mind the above findings and statements one may proceed to the following indicative approach to estimate and characterize certain micromagnetic state-coupled microstructural parameters. First of all, for simplicity of this approach, it is assumed in Eq (27) that m << 3/2 (or p >> 2/3) which would mean a negligible influence of wall mobility on J-parameter associated with a high, pinning strength as well as high pinning density fact, equivalent with a reduced pinning spacing, l. Thereafter, from the J-strain curve of Fig (5) one may extract the following specific magnetic values related to the strain: $J_{0,1\%} \approx 0{,}08$ and $J_{1\%} \approx 0{,}092$. The first value corresponds to the microyielding strain of 0, 1% and second one to the progressive yielding of 1% strain at which cell-

formation sets on [19]. Next, using Eq (27) one can obtain the ratio.

$$J_{0,1\%}/J_{1\%} = \left(l_{0,1\%}/l_{1\%}\right)^{3/2} \cdot \left(\tilde{q}_{0,1\%}/\tilde{q}_{1\%}\right) = 0{,}08/0{,}092 \cong 0{,}81 \quad (30)$$

Using the earlier established linearity of j with strain, dueto dominating effect of the $\tilde{q}-$ factor, one may suggest $\tilde{q} \propto \varepsilon\%$ and as such $\tilde{q}_{0,1\%}/\tilde{q}_{1\%} \approx 1/10$ which leads to the finally basic result:

$l_{0,1\%}/l_{1\%} \approx (8)^{2/3} \approx 4 > 1$ which means $l_{1\%} \ll l_{0,1\%}$.

It is mentioned that the above give strain value of 0, 1% corresponds to the early deformation stage of microyielding where dislocation motions and multiplications are vanishing. Consequently, this stage can be seen as a state of an initial pinning spacing equivalent to the average grain size of steel, i.e. $l_{0,1\%} \approx 30\mu m$. Thereafter, from the above relationships, one way deduce that under conditions of early stages of plastic deformation and within the prenecking range, the initial-nominal pinning spacing is reduced at least to about $30/4 \approx 8\mu m$, fact which means that during this strain range, formation of fresh dislocation-aided pining sites should occur within the crystal grains of iron. Now, the behavior of the J-curve beyond the characteristic stain point,$\tilde{E}_{cr}$, needs, and within the postnecking I*-region some different interpretations and explanations. At this point, as above-mentioned, high triaxial tensile stress fields develop by producing volumetric damages within the formed cell areas. These damages act as additional pinning sites for domain walls in reducing the effective pinning spacing, l, and increasing pinning strength and hence reducing the wall mobility number, m. Furthermore, an increase in the triaxial tensile stresses facilitates a relative increase in the complementary (secondary) transverse domain walls population, anchored to the basic-longitudinal domains. This, in turn, facilitates an increase in the magnetostrictive friction which means larger bulging deflections, i.e. larger bulging strength numbers, b in Eq (28). Consequently, according to this, the combined effect of a rapid decrease in, l_{eff} and a (modest) decrease in wall mobility number, m, seems to dominate over the flow stress elevation factor $\tilde{q}$-effect resulting in a net decrease in the obtained J-curve of Fig (5). Thus, this behavior can be correlated to with an associated increase in the magnetic hardening of the material [5, 13, 14]. At this place it should be pointed out, that the magnetic measurements were conducted by holding as far as possible, the pick-up probe within the necking region, thus minimizing elastic unloading effects caused by necking instability phenomenon.

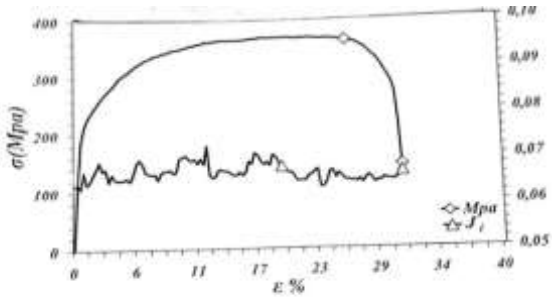

Figure 6: Mechanical stress-strain and magnetic J – response curves for 200 hours of corrosion time

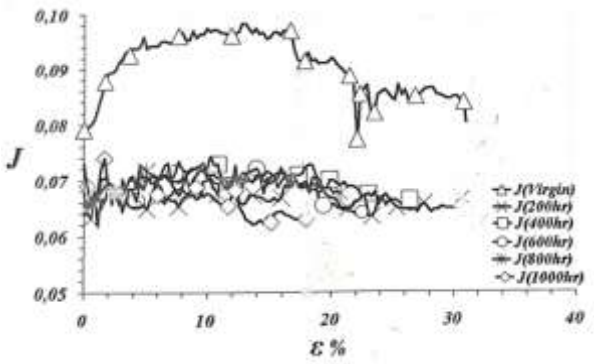

.

Figure 7: Changes in the J-parameter in function of applied strain for specimens corroded for different times.

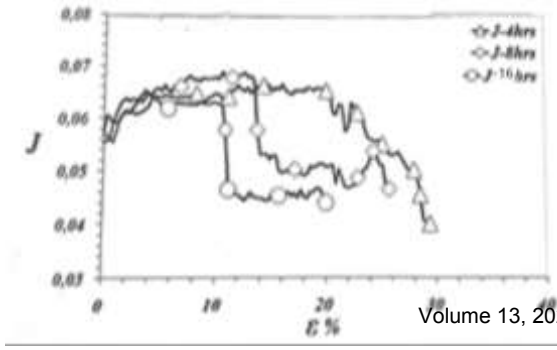

Figure 8: Changes in the J-parameter in function of applied strain for specimens of different times of isothermal heating.

In Fig (6) and (7) the obtained magnetic J-strain curves for untreated (virgin) and treated specimens after their exposure to corrosive NaCI- water solution for increasing given times are presented. By the way, one

can demonstrate that iron exposed to solt-water solution may be subjected to hydrogen-induced microstructural degradation [8,13,20,21] . Thus, one can clearly observe the overall large, drop-like shift of all curves of treated specimens to lower values of s.m.a.- J compared to untreated specimens. This behavior should clearly be related with an associated hydrogen-assisted magnetic hardening effect occurred by corrosion in steel [5, 13, 14], fact which, in a more or less phenomenological way, may shortly be explained as follows: atomic hydrogen, by diffusion, is preferably accumulated at internal stress gradient sites and/or other microstructural defects [20]. In this manner two major competitive hydrogen-assisted effects occur; first, stress relief and second void initiation and growth [20]. For the micromagnetic activity the first leads to an attenuation of cell-flow stress elevation $\tilde{q}$ −factor and the second to a decrease in the pinning spacing, l, in Eq (27). Consequently, according to this equation the above mentioned large shift of the curves of treated specimens to lower J-values should be attributed to a related increase in the magnetic hardening [5, 13, 14].

Thereafter, one can also observe in Fig (7) that for 'critical' times of exposure larger than about 200hrs, the mentioned hydrogens effects tend to attenuate toward a limiting overall magnetic hardening. This behavior could be attributed, at first, to an exhaustive void production and hence a pinning spacing reduction. An additional explanation for the above observed 'collective' large shift of J-curves to lower magnetic values may , in short, be given an the basis of a kinematics- aided approach presented by the authors in a previous study [15]. as fallows: since the stress-relief effect can dominate over that of void creation [20], it follows that the rate of reduction in the wall start acceleration, $\tilde{a}$, is dominating larger than that of reduction in the pinning spacing, l. Thus, due to the kinematic equilibrium of rate of changes of all variables in Eq l=$\tilde{a}t^2$/2, a correlated net increase in the traveling time, t, should result.

Furthermore, since pinning spacing reduction leads to a related reduction in the magnetic volume changes, B, by virtue of the relationship Vrm &B/t, a associated reduction in the induced voltage should result , fact which , in turn , by virtue of Eq J =Vrms/N, leads to a net decrease in the needed $J-$ parameter . (Void creation causes an increase in the number of pinning sites density n and hence would lead to a decrease in the above J -ratio).

In Figure (8) the specific magnetic data obtained for specimens subjected to isothermal heating –tempering treatment at 440 $C^0$for given processing times are presented. It is known that in steels, cooled slowly or isothermally heated in the temperature range of 400 C^0 to 600C^0 an embrittlement takes place [22].

It is in general accepted that such embrittlement is a result of segregation of impurity elements (atoms) at prior austenitic grain boundaries and various internal stress-strain gradient sites. Such embrittling elements may be P, As, Sn, Sb e.t.c. Although the actual mechanism for temper embrittlement remains unclear, it is believed that segregation of impurities may substantially reduce the atomic cohesive bonding energy of lattice at these sites [22].This, in turn, lowers the critical local stress necessary to generate volumetric damage sites in creating new internal (free) surfaces fact which leads to premature-unexpected degradation of material.

At the same time, during isothermal heating in this temperature range, a so – called recovery process takes place, which is a multistage process including all the elementary processes taking place prior to recrystallization [19]. Recovery should be understood as a process of microstructural perfection of a metal by redistribution and annihilation of point defects, as well as, by redistribution and partial annihilation of dislocations. During this process a reduction of internal stresses by stress relaxation in the elastically distorted regions occurs , due to thermally activated shear when the yield stress at given temperature becomes lower than the elastic strain produced by dislocations [19]. In the above mentioned figure one can clearly observe, that beyond a certain characteristic strain point an overall drop-like decrease in the J -curve arises. As it was shown in previous studies [5, 13, 14], this strain point almost coincides with the ultimate strength point of the tensile engineering stress-strain curve. Thus, at this point a plastic instability phenomenon takes place by necking formation in the tested specimens. This, in turn, is related with a rapid creation of volumetric internal damage sites in form of voids, dimples, cavities and microcracks. Consequently the creation of such damages at ultimate tensile strength point is strongly enhanced by the above – mentioned temper processing effects. The damages created in this way act as additional pinning sites in reducing the pinning spacing l. Nevertheless, due to large flow stress restriction, the $\tilde{q}$- factor effect is also reduced. The reduction in the both parameters, l and$\tilde{q}$, leads, according to eq (27), to a rapid reduction in the J -parameter.

Thereafter, the formation of drop- like decrease in the curve observed for larger tempering time, 8 and 16 hrs, should be attributed to an intensive and very rapid segregation of atomic impurities at defect sites thus leading to a drop-like decrease in the J-curves. The above –described behavior is related with an increase in the magnetic hardening tendency of material fact which means that the larger is the drop the higher results to be the magnetic hardening degree. In this sense, a larger shift to lower J -values of the temper curves compared to the corrosion curves of Fig (7) can be distincted. This means that tempered specimens are subjected to an increased magnetic hardening compared with Na-Cl corroded one. Furthermore, the more or less, stabilized- horizontal evolution behavior of the J-curves observed for 8 and 16 hrs, of tempering beyond the critical drop- point could be attributed to a balance of reduction in l and ,this time, an increase in the $\tilde{q}$-factor effect due to the existence of high triaxial tensile stresses in the necking region. Moreover, the absence of such large drops of decrease in the corrosion curves of Fig (7) may be attributed to the fact that temper effect seems to exert a stronger influence on the magnetic properties of steel compared to hydrogen effects. This is because of larger difference of embrittling species, hydrogen and phosphor, fact which by segregation – accumulation, large- sized species cause associated large volumetric damage. An additional explanation for the observed lower J-value of temper specimens compared to corrosion ones, can be given by kinematics- aided approaches [15] as follows:

Temper processing causes intensive stress gradient relaxation due to dislocation redistribution and strong bounding energy reduction effect. This would cause, compared to corrosion, respective larger reductions in the pinning strength (force), and hence in the wall start acceleration of domain walls. As such, by virtue of kinematic counterbalance in equation, $l = \tilde{a}t^2/2$, and bearing in mind that pinning spacing changes in tempering and corrosion due not differ substantially , a correlated larger net values of travelling time ‘t’ should result in tempering . In turn, it results that pinning spacing- controlled magnetic volume change in ‘B’ also not differ substantially, and as such from relationship Vrms ∝B/t , a lower value of the induced

voltage results in tempering. Thus, finally, by equation J=Vrms/N a lower net value of s.m.a. should be expected in tempering. This is because pinning density, n, or count rate N, increases with decreasing pinning spacing.

5. Conclusion

The semiquantitative analysis presented in this study may help to give more detailed and plausible explanations concerning the complex interplay between micromagnetic activity and deformation – assisted microstructural changes in a mild steel under condition of applied stress and various physico- chemical degradation factors investigated by means of data obtained from micromagnetic Barkhausen emission measurements. As such, by adequate functional relationship, approaches, developed in this direction , a specific micromagnetic activity (s.m.a.) parameter was introduced by which the combined – opposite effect of microscaling parameters such as cell size – controlled pinning spacing and internal cell – flow stress on the micromagnetic activity may reasonably be revealed , analysed and explained. In this context the stimulating effect of internal cell-flow stress in increasing the s.m.a- parameter and the depressive effect of the cell-size reduction in decreasing this parameter with plastic deformation can also be revealed and analyzed. The dominance of the internal cell- flow stress in increasing the s.m.a. – parameter within the prenicking deformation range can be demonstrated.

Nevertheless, the dominance of damage-assisted cell size and pinning spacing reduction effect in decreasing the s.m.a. parameter within the postnecking deformation zone, may also reasonably be explained.

By using the adequately developed functional approaches, the influence on the s.m.a. - parameter of certain environmental degradation factors such as temper processing and electrochemical corrosion of material exposed to NaCl- water solution can also, in a semiquantitative way, be revealed and analysed. Thus, one can demonstrate, that the physico-chemical degradation factors such as hydrogen, introduced by solt-water corrosion, and impurities segregation introduced by tempering processing , may lead to a substantial reduction in the s.m.a. – parameter. By this reduction an associated embrittlement as well as a magnetic hardening of steel occur. The needed explanations are given on the basis of compenting effects of cell-size- controlled pinning spacing and pinning strength on the micromagnetic behaviour. With respect to this, due to larger cell- flow stress restrictions occurring in tempering, determined by impurities segregation-induced critical- local fracture stress reduction, an increased magnetic hardening in tempered specimens compared to corroded ones appears. Within the fraim of the obtained findings the used functional approaches seem to be able to give plausible semiquantitative explanations of measurement data.

Appendix-A

Generally, it is known that [22]:

$$6_\infty = H \cdot \varepsilon^n \qquad \text{(A-1)}$$

Specifically, one may assume:

$6_o \rightarrow 6_f = H\tilde{e}^n$ =internal cell flow stress (A-2)

And further one may obtain

$$\frac{d6_o}{d\tilde{e}} \rightarrow \frac{d6_f}{d\tilde{e}} \cong Hn\acute{e}^{n-1} = \bar{R}_o \qquad \text{(A-3)}$$

and also:

$$\frac{6_\infty}{\acute{\varepsilon}} = \bar{R}_\infty \qquad \text{(A-4)}$$

$\bar{R}_o$ = average strain hardening rate and $\bar{R}_\infty$ = average rate of change in the (remote) applied stress with strain of cell formation. It is further assumed that the overall plastic

strain range of extensive cell formation $\tilde{\varepsilon} = (2-18)\%$ and as such the given average strain value of cell formation $\acute{\varepsilon} \cong 10\%$. Bearing in mind these data and that for mild iron$H \approx 500MPa$, $n \approx 0{,}11$ [22] one may finally approximate:

$$\bar{R}_o/\bar{R}_\infty \approx 1/6 \qquad \text{(A-5)}$$

Consequently, one can reasonably assume that6_o, changes slowly compared to applied stress,6_∞, and hence changes also slowly with plastic strain- induced cell size reduction and as such the first (6_0) may be taken as a constant parameter in the related relationships in the text.

Furthermore, the proposed internal cell-flow stress may roughly be correlated with the dislocation tangles density of cell-wall formation as$6_o \propto \sqrt{S_t}$, where S_t is the dislocation density in the cell wall [9]. The later seems to increase not substantially with plastic deformation [9] and hence with cell size. Thus, 6_o should, ones more, be taken as a constant parameter in the related relationships in the text.

APPENDIX-B

For the count rate emission one can choose, as far as possible, simple functional approaches in function of wall mobility, m, and /or pinning strength, p, as given by:

$$N_m = \frac{6_\infty}{6_0}\xi_o\left(\frac{1}{l}\right)^m \quad \text{and} \quad N_p = \frac{6_\infty}{6_0}\xi_o\left(\frac{1}{l}\right)^{1/p} \qquad \text{(B-1)}$$

Thus, the validity of the following condition should exist:

$N_m = N_p = N$= average measured count rate which means:

$$\frac{6_\infty}{6_y}\xi_o\left(\frac{1}{l}\right)^m = \frac{6_\infty}{6_y}\xi_o\left(\frac{1}{l}\right)^{\xi_{m,p}} = \text{N} \qquad \text{(B-2)}$$

with m=f_m (l) and p=f_p(l) as a wall mobility and pinning strength function respectively

It results that

$f_m(l)\cdot f_p(l) = \xi_{m,p}$= functional correlation factor of microstructural pinning state.

One can further assume a simple functional relationship between wall mobility and pinning spacing as given by expression:

$$f_m(l) = a\cdot l^\beta, (a,\beta \le 1) \qquad \text{(B-3)}$$

As such, the following microscaling functional relationship approach should result for the count rate function:

$F_N(l) = (1/l)^{a^{l^\beta}}$, from which one can easy find $l_{max} = 1/e^{1/\beta}$ and also by L' Hospital limit law one may calculate:

$$\lim_{l\to o} F_N(l) \to \infty^o \to 1 \qquad \text{(B-4)}$$

Thus, by means of the above assumptions the following schematic sketch may be constructed:

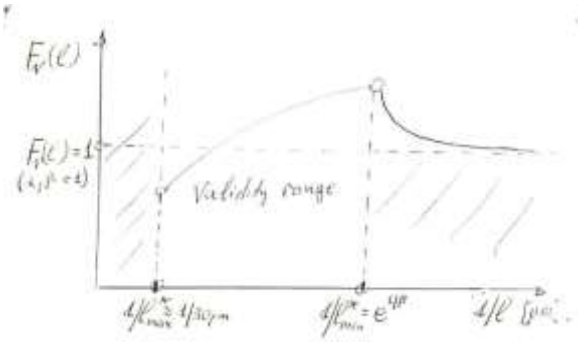

Figure (9), Schematic of 'suppressed' parabolic increase in the count rate function (F_N) with decreasing cell size.

Thus, In this schematic presentation an equivalent, the parabolic increase in the count rate in function of the decrease in the cell size parameters, l. can be simulated. Thereafter, one can establish:

$$l_{min} \ge \acute{e}^{1/\beta} \ge \frac{1}{e} \approx 0{,}35\mu m \qquad \text{(B-5)}$$

This means that the final condition of validity of the related approach should be given as: 0, 35 μm ≤ $l \le 30\mu m$= grain size.

With respect to this validity condition it is worth noting that the evaluated low limit value of cell size, $l_{lim} \cong 0{,}35\mu m$, is not dissimilar to the smallest cell size values observed in fine-grained iron after progressive plastic deformation [19].

References

[1] Mohamad Blaow, Jahn Terence and Brian A. Shaw, "The effect of microstructure and applied stress on magnetic Barkhausen emission in induction hardened steel, J. Mat. Sci. Val 42, p. 4364-4371, (2007).
[2] C. E. Stefanita, L. Clapham and D. L. Atherton, "Subtle changes in magnetic Barkhausen noise before the macroscopic elastic limit" J. Mat. sc. 35, p 2675-(2000).
[3] Thomas W. Krause, L. Claphan, Andreas Pttantyus and Davied L. Atherton," Investigation the stress- dependent magnetic easy axis in steel using magnetic Barkhausen noise". J. Appl. phys. Vol. 79 (8), 15 April 1996, p 4242-4252.
[4] D. C. Jilles and D. L. Atherton, "Theory of the magnetization process in ferromagnets and its application to the magnetomechanical effect" J. Phys. D., 17 (1984), p. 1265 – 1281.
[5] V. N. Kytopoulos, A. Altzoumailis, Chr. Panagopoulos, Chr. Riga. "Hydrogen influence on certain mechanical and magnetic properties of a stressed Low-Carbon Steel after Corrosion in NaCl-water solution", Procedia Structural Integrity 26 (2020), p. p. 113-119. www.sciencedirect.com
[6] D Gwang and H C Kim. The influence of plastc deformations on Barkhausen effects and magnetic properties in mild steel Journal of Phys D applied physics, 1988 21 p 1807 – 1813.
[7] Tadao Nozawa, Masato Mizogami, Hisai Mogi and Yukio Matsuo, 'Domain structures and magnetic properties of advanced grain- oriented silicon steel" J. Magn. Mater. 133, (1994) p. 115-122.
[8] E. K. Ioakeimidis, V. N. Kytopoulos, E. Hristoforou "Investigation of magnetic, mechanical and micro failure behavior of ARMCO – type low carbon steel corroded in 3.5%NaCl-aqueous solution" - Materials Science and Engineering: A, Volume 583, 2013, p 254-260.
[9] J. Degauque, B. Astie and L. P. Kubin,"Evidence for Interaction between Magnetic domain walls and Dislocations in high-purity Iron from Magnetomechanical damping measurements." Phys. state so. (a), 45, p 493-501 (1978).
[10] Martha Pardavi-Horvath, "Magnetic Noise Barkhausen Effect "in Wiley Encyclopedia of Electrical and Electronic Engineering, Val. 12, p. 52-64, y. E. Webster Ed., 1999.
[11] A. Hubert and R. Schäfer: "Magnetic Domains: The Analysis of Magnetic Microstructure", Springer, Corrected Printing 2000.
[12] S. Chikazumi, Physics of Ferromagnetics, Oxford, Science Publications Reprint 2005.
[13] A. F. Altzoumailis, V. N. Kytopoulos, "On Novel Aspects of Hydrogen Effects on Applied Stress - Coupled Micromagnetic Activity in a Mild Steel after Exposure to NaCl – Water Solution: A Combined Approach", International Journal of Materials Dol: 10.46300/91018.2021.8.4. Volume 8, 2021
[14] A. F. Altzoumailis, V. N. Kytopoulos, "Characterization of a mild steel by its mutual Tensile Mechanical and Micromagnetic emission response after corrosion in NaCl – water Solution: a combined semiquantitive approach" International Journal of MaterialsDol: 10.46300/91018.2021.8.3. Volume 8, 2021
[15] A. F. Altzoumailis, V. N. Kytopoulos, "On modelling approaches to the influence of mechanical deformation on the micromagnetic activity in a mild steel "International Journal of Materials DOI: 10.46300/91018.2021.8.3. Volume 8, 2021.
[16] O. Saquet, J. Chicois, A. Vincent,"Barkhausen noise from plain carbon steels: analysis of the influence of microstructure "Mat. Sei. Eng. A, pp 73-82, (1999).
[17] V. N. Kytopoulos, A. F. Altzoumailis: "Unpublished data "School of applied Math. And Physic Sciences, NTUA-Greece, 2015.
[18] S.M. Thomson, B. K. Tanner," The magnetic properties of specially prepared pearlitic steels of varying carbon content as a function of plastic deformation",J. Of Magnetism and Magnetic Materials, 132, 71-88, (1994).
[19] P. Polukhin, S. Gorelic and V. Vorontsov, "Physical Principles of Plastic Deformation", (in English), Mir Publishers, Moscow. 1983.
[20] C. L. Briant, "Metallurgical Aspects of Environmental Failures", Materials Science Monographs, Vol 12, Elsevier, 1985.
[21] A. K. Das, "Metallurgy of Failure Analysis", Mc Graw – Hill, 1996.
[22] R. W. Hertzberg "Deformation and Fracture Mechanics of engineering materials" 3d Ed., Willey, 1989.